Ocean Engineering
May 2023, Volume 276 Pages 114116 (11p.)
https://doi.org/10.1016/j.oceaneng.2023.114116
https://archimer.ifremer.fr/doc/00828/93999/

Semi-analytical load models describing the progressive immersion of a fixed vertical cylinder in a breaking wave

Renaud Paul [1, 2, *], Martin Marc Batlle [1, 3], Hulin Florian [1, 2, 4], Harris Jeffrey C. [3], Filipot Jean-François [1], Scolan Yves-Marie [2]

[1] France Energies Marines, Plouzané, France
[2] ENSTA Bretagne, CNRS UMR 6027, IRDL, Brest, France
[3] LHSV, Ecole des Ponts, EDF R&D, Chatou, France
[4] IFREMER, Plouzané, France

* Corresponding author : Paul Renaud, email address : paul.renaud@france-energies-marines.org

Abstract :

This paper is part of the DIMPACT (Design of floating wind turbines and impacts of energetic steep and breaking waves) project concerning slamming loads on floating offshore wind turbines. Two semi-analytical models accounting for the progressive immersion of a vertical cylinder in a breaking wave are presented. These models are based on the rate of change of the fluid momentum and the continuity of the added mass during immersion. The first model is based on the Generalized von Kármán Model where the real shape of the body and its added mass are accounted for. To account for the nonlinearity of the flow kinematics, the second-order terms of the momentum equation are considered in the inertia load. The total load is obtained by adding the drag force using a variable drag coefficient. To better predict the slamming load, a second model based on Wagner's theory is presented. The Modified Logvinovich Model provides the pressure distribution at the first instants of impact. It is assumed that the flow does not separate from the structure. The load models are applied in a strip-theory approach under the Froude–Krylov assumption. For comparison, a Navier–Stokes solver is used to generate four phase-focused breaking waves. The resulting free surface shape and the ambient kinematics of the two-dimensional waves are used in the semi-analytical models. The present models are compared with existing slamming load formulations and a three-dimensional numerical simulation with an actual cylinder, where the load on four sections of the cylinder are considered. The force in the deeply immersed sections is in good agreement in all models considered. In the partially submerged section, the proposed load formulations and the three-dimensional simulation predict a similar load. Other standard engineering formulas predict a much lower force in this section. In the area impacted by the crest, the Froude–Krylov-based approaches predict a much higher force than that given by the Navier–Stokes result, likely due to the free surface being disturbed by the cylinder.

Highlights

► The extreme wave loads acting on a vertical cylinder are studied using semi-analytical models. ► The models are applied in a strip-theory approach using the actual free surface shape and the kinematics of undisturbed waves. ► The present models are compared with other formulations and numerical results. ► The ability of the models to predict the load in partially submerged strips is demonstrated.

Keywords : Breaking wave, Vertical cylinder, Wave loads, Slamming, Progressive immersion

1. Introduction

1.1. Context

The growing demand for energy, the climate emergency, and the dramatic drop in cost of offshore wind energy has resulted in dramatic increases in offshore wind industry development. Offshore wind turbines are often installed in harsh environments leading to extreme aerodynamic and hydrodynamic loads. Loads induced by breaking waves, also known as "slamming loads" may represent a significant part of the extreme hydrodynamic loads and must often be considered in the Ultimate Limit State (ULS) design of offshore wind turbines. Indeed, the hydrodynamic load associated with a slamming event generates a significant peak force that can damage the structure. Reducing uncertainties of the calculated slamming forces related to breaking waves is the goal of the present paper, and is part of

the DIMPACT (Design of floating wind turbines and impacts of energetic steep and breaking waves) project led by France Energies Marines. The project aims to refine the assessment of extreme steep and breaking wave loads on floating offshore wind turbines.

There are mainly two methods to empirically predict the hydrodynamic load induced by breaking waves on offshore structures. In the first approach, the total load is divided into a quasi-static load induced by the non-breaking part of the wave and an additional slamming load. In this case, the formulas for the slamming load generally depend on a low-fidelity description of the wave (Goda et al., 1966; Wienke and Oumeraci, 2005; Alagan Chella et al., 2012; Paulsen et al., 2019). In the second approach, the force depends on the progressive immersion of the cylinder in the fluid, in which the slamming part is taken into account in the partially immersed portions of the body. A high-fidelity description of the wave is then considered in a strip-wise manner (Nestegård et al., 2004; Hansen and Kofoed-Hansen, 2017). The different models to calculate the wave load acting on a structure piercing the surface are described below.

The quasi-static horizontal load on a fixed vertical cylinder is usually computed with the classical Morison equation (Morison et al., 1950). In the DeRisk project (Bredmose et al., 2016), different Morison-type formulations were compared for steep and breaking waves (Suja-Thauvin et al., 2020). When accounting for second-order kinematics of the flow, the Lagrangian acceleration, and the axial divergence term (Manners and Rainey, 1992) are involved in the distributed load. The Morison "FNL" Fully Non-Linear formulation extends the Morison equation by taking into account the nonlinear wave kinematics. In Pierella et al. (2019), as part of the DeRisk project, the quasi-static load is computed with the Rainey model (Manners and Rainey, 1992; Rainey, 1989). This load formulation assumes the conservation of the kinetic energy as the wetted surface of the cylinder expands and takes into account the contribution of the partially immersed portion of the cylinder. The effort acting on the immersed part can be significant for steep waves. The Rainey model, to the best of our knowledge, is the only quasi-static wave load model accounting for the contribution of the partially immersed strips.

With the Morison formula, the drag load is added to the inertia load, which is particularly important when a boundary layer appears. This is the case when the velocity becomes small enough, in particular in the lower parts of the cylinder where the wave effects are dampened. When the cylinder is fully submerged, the drag coefficient is constant with typical values ranging from 0.60 to 1.2 (El-Reedy, 2012), depending on the Reynolds number of the flow. In Zhu et al. (2005), a formulation of the drag coefficient as a function of the penetration depth of the body in the fluid is obtained from the experimental work of Sarpkaya (1966). Sarpkaya's experiments were conducted in an essentially infinite fluid, with an impulsive start. Although the free surface could affect the drag force in some way, for modeling the hydrodynamic force during the progressive immersion of the body in the fluid, this formulation can still be used.

The inertia force is normally calculated with a constant coefficient, with typical values for a circular cylinder in the range of 1.5-2 (El-Reedy, 2012). However, as shown in Clément et al. (2022), the horizontal force in the area close to the free surface drastically decreases when approaching the air/water interface. Thus, for steep and breaking waves, a variable inertia coefficient depending on the position with respect to the free surface would be more appropriate.

The additional slamming load due to a wave breaking on a structure is commonly calculated under the assumption that the front of the wave is vertical. The two-dimensional equivalent is the impact of a horizontal cylinder on a flat free surface without gravity, which has been studied quite extensively and many time-varying slamming coefficients have been established or calculated (see Alagan Chella et al., 2012, for an overview). The hydrodynamic impact was first studied by von Kármán (1929) to quantify the impact load during the landing of a seaplane. The theory is based on the conservation of momentum and a linearization of the free surface and the body shape, which is assumed to be a flat plate. For a circular cylinder impacting a flat free surface the slamming coefficient is $C_s = \pi$. The hydrodynamic impact problem was extended by Wagner (1932), including the pile-up effect. Using the linearized Bernoulli equation and the flat plate approximation, the slamming coefficient of a circular cylinder impacting a flat free surface is then $C_s = 2\pi$, known as the Linearized Wagner Model (LWM). Both models can be generalized by accounting for the real shape of the body, leading to the Generalized von Kármán Model (Malenica and Korobkin, 2007) and the Generalized Wagner Model (Zhao et al., 1996). Comparisons between the experiments from Campbell and Weynberg (1980); Cointe and Armand (1987), show that analytical asymptotic models based on Wagner's theory are the most accurate for the first instants of penetration of the body into the fluid (Korobkin, 2004; Tassin et al., 2010). However, Wagner's theory is based on the integration of the pressure field derived from the Bernoulli equation and at the leading order, the pressure predicted by the LWM is singular.

Pressure distribution formulations such as the Modified Logvinovich Model (MLM) (Korobkin, 2004) allow com-

puting a uniformly valid distribution of pressure up to the boundary of the wetted surface. The MLM considers the quadratic term of the Bernoulli equation and the real shape of the body by extrapolating the pressure and the velocity potential via a Taylor expansion on the body surface. In its original version, the total pressure from the MLM is integrated on its positive support. In Tassin et al. (2013); Korobkin et al. (2014), it is proposed to integrate the term proportional to the velocity squared only over its positive support. The resulting force can then be decomposed into a first term proportional to the acceleration and a second proportional to the velocity squared. This is done in Korobkin et al. (2014), where the slamming force of three impact models (Original Wagner Model, Modified Logvinovich Model and Generalized Wagner Model) are evaluated under this decomposition. This decomposition is similar to the time rate of change of momentum formulation involving the added mass of the body which is the basis of the von Kármán model. This work has recently been extended to account for gravity effects in Sun et al. (2022). Nevertheless, the Wagner Model is only valid at the first instants of penetration of the body in the fluid, and can not be used till the full submersion of the cylinder. One way to extend Wagner's theory up to the flow separation and after, is the Fictitious Body Continuation (FBC) method, introduced by Tassin et al. (2014). The water entry of different symmetric (Tassin et al., 2014) and asymmetric geometries (Hascoët et al., 2019) after flow separation show very good agreements with experimental and numerical results. Thanks to the principle of the FBC method, the penetration depth for which the separation occurs can be determined.

The slamming load induced by breaking waves acting on a vertical cylinder was first studied by Goda et al. (1966), based on von Kármán's theory. It was then extended by using Wagner's theory by Wienke and Oumeraci (2005), during the Wifi JIP Project (Ridder et al., 2017) and by Paulsen et al. (2019). In these formulations and in the general expression proposed by Alagan Chella et al. (2012), the two-dimensional impact load is assumed to be uniform over the wave height involved in the impact. These expressions account for a low-fidelity description of the breaking wave. The slamming load depends on the breaking phase speed while the horizontal fluid velocity is actually not uniform in the wave. Also, the free surface shape is defined only by the curling factor, which indicates the proportion of the wave height contributing to the impact. Indeed, this quantity is difficult to quantify. Paulsen et al. (2019) were able to establish an empirical formula of this parameter based on the observations of breaking waves in irregular waves, generated experimentally. Wienke and Oumeraci (2005) measured loads of large-scale phase-focused waves. A maximum curling factor of $\lambda = 0.46$ was found for the vertical cylinder, which is consistent with the referenced values from Goda et al. (1966) ($\lambda = 0.4$ - 0.5). As observed during the Wifi JIP Project, phase-focused waves have a higher curling factor than standard irregular waves (the mean λ is 0.56 for focused waves versus 0.23 and 0.36 for flat seabed waves and sand waves respectively). The waves generated in this study to compare the different load models are phase-focused waves, but there is no specific criterion to estimate the curling factor on this type of wave.

One way to avoid the curling factor and to account for the vertical variation of the horizontal velocity in the crest is to consider the hydrodynamic impact in a strip-theory approach. This is done in Nestegård et al. (2004). The slamming load is taken into account by considering the progressive immersion of the cylinder. From the early stage of penetration until the full immersion of the strip, the load is estimated with the empirical formula from Campbell and Weynberg (1980). This formula describes the water entry of a horizontal cylinder on a flat free surface at constant speed and accounts for flow separation at large penetration depths. When the penetration depth reaches the diameter, the cylinder is fully immersed. The hydrodynamic load is then computed with the classical Morison equation. Constant drag and inertia coefficients are used in Nestegård et al. (2004). This method is referenced in the standard practices (DNV, 2021) to compute the load from steep near-breaking waves. A similar method is presented in Hansen and Kofoed-Hansen (2017), but Goda's formula is used to account for slamming loads. In Hansen and Kofoed-Hansen (2017), the load acting on the fully immersed strips is computed with the Morison equation as well. The inertia coefficient derived from the linear wave diffraction theory (McCamy and Fuchs, 1954) is implemented. In Nestegård et al. (2004); Hansen and Kofoed-Hansen (2017), the free surface elevation of experimental waves is measured, but the wave kinematics is approximated or stretched using the Wheeler model. Also, in Nestegård et al. (2004) and in Hansen and Kofoed-Hansen (2017), the fluid velocity is assumed constant in the partially immersed strips and the load model is abruptly changed at full immersion.

The method presented in Kaplan and Silbert (1976); Sarpkaya (1978); Khalil and Ali (1994); Prasad (1994); Akter (2011) proposes a continuous formulation of the inertia hydrodynamic load during the immersion of a horizontal cylinder in the fluid. The time rate of change of momentum involving the added mass of a circular cylinder near a free surface (Greenhow and Ahn, 1988) is used to compute the progressive immersion of the body. The inertia hydrodynamic force in a cross-section of the cylinder accounts for the time variation of the added mass in terms of

submergence.

In search for a continuous formulation of wave loads during the immersion of the structure, the approach used to model the immersion of a horizontal cylinder is followed for a vertical cylinder. The actual shape of the body and its corresponding added mass are accounted for. In order to account for the highly nonlinear nature of breaking waves, quadratic terms in the momentum equation are added. For deeply immersed parts of the cylinder where the added mass no longer varies, the inertia load returns to that of a Morison-type formulation. The total force is obtained by adding the drag force with a variable drag coefficient depending on the immersion depth. To better predict the load during the early stages of impact, a second model based on Wagner's theory is presented. The pressure distribution from the MLM is integrated on the wetted surface of the body. The major assumption of this second model is that the flow does not separate from the body. Since the MLM can not be used until the body is fully immersed without flow separation, the added mass predicted by the integration of the MLM is linearly interpolated to the added mass predicted under the Generalized von Kármán Model. By using this second model, the hydrodynamic impact in the frame of Wagner's theory is accounted for in every strip of the cylinder. This avoids the assumption of a curling factor. To account for the real free surface shape and the vertical variation of the wave kinematics, the models are applied in a strip-theory approach. Numerical waves are generated using Computational Fluid Dynamics (CFD). The kinematics and shape of focused breaking wave packets are derived from a Navier-Stokes solver (Batlle et al., 2022). There are 2 configurations: one denoted 2D (two-dimensional) since the presence of the body is not accounted for, and the other denoted 3D (three-dimensional) because the perturbation of the vertical cylinder is taken into account.

The paper structure is as follows. The theoretical models are introduced in section 2. Two models are presented: one is based on the Generalized von Kármán Model and the second is based on the MLM and the continuity of the added mass during immersion. The proposed models account for the shape and kinematics of numerical phase-focused breaking waves. The results from the present formulations are compared in section 3 with a 3D configuration including a vertical cylinder and with other common formulas. A discussion is then proposed in section 4.

2. Semi-analytical wave load models

The purpose of the present development is to propose a continuous formulation of the hydrodynamic load acting on a strip from the early stages of penetration until the full submersion. Variable hydrodynamic coefficients with respect to the penetration depth are used to compute the inertia and the drag load.

2.1. Inertia hydrodynamic load

The distributed inertia hydrodynamic load acting on an elongated fixed body is expressed as follows:

$$dF_i = \left(\rho A \frac{dU}{dt} + m_a \frac{dU}{dt} + \frac{dm_a}{dh} U^2\right) dl \tag{1}$$

with dl the thickness of the strip on which the force dF_i is calculated. A is the cross-sectional area of the immersed part of the body, U is fluid velocity in the same direction as dF_i. m_a is the two-dimensional added mass of the body and h is the penetration depth of the strip with respect to the free surface. The first term on the right-hand side in Eq. 1 represents the inertia hydrodynamic load due to fluid volume displaced by the body. The second and third terms represent the time-rate of change of fluid momentum.

In this first proposed semi-analytical model, m_a is computed in the frame of the Generalized von Kármán Model. There is neither wetted correction nor linearization of the body boundary (see Fig. 1 for illustration). The added mass of a partially immersed cylinder near a free surface is well-known (see Fig. 2 in Greenhow and Ahn, 1988).

The variation of the immersed section area A of a circular cylinder with respect to the penetration depth is

$$A = \frac{R^2}{2}[\beta - \sin(\beta)] \tag{2}$$

with

$$\beta = 2\arccos\left(1 - \frac{h}{R}\right), \text{ for } 0 \leq \frac{h}{R} \leq 2 \tag{3}$$

2.2. Consideration of the nonlinearities of the kinematics of the flow

At this stage of the modeling, the inertia load acting on the deeply immersed strips (for $h \gg R$, $\frac{dm_a}{dh} = 0$ and $\frac{m_a}{\rho\pi R^2} = 1$ (see Greenhow and Ahn, 1988)) is similar to the inertia force predicted by the classical Morison equation (Eq. A.1).

As breaking waves are highly nonlinear waves, nonlinearities are introduced with the second-order kinematics of the flow. The fluid acceleration accounts for the convective terms (Eq. A.3). The axial divergence term (Manners and Rainey, 1992) given by $dF_{ad} = m_a U W_{,z} dl$ is added to the distributed load. W is the vertical fluid velocity. The vertical derivatives $U_{,z}$ and $W_{,z}$ are calculated from one strip to another by using 1^{st} order finite difference scheme.

For deeply immersed strips, the inertia load model reduces to the Morison FNL model (see Eq. A.2). The gradients of the fluid velocity are involved. They increase rapidly near the free surface when the wave becomes steep.

Finally, the distributed inertia hydrodynamic load is

$$dF_i = \left(\rho A(h)\frac{dU}{dt} + m_a(h)\frac{dU}{dt} + \frac{dm_a}{dh}U^2 + m_a(h)UW_{,z}\right)dl \tag{4}$$

2.3. Drag force

The full expression of the load is obtained by adding the drag force with a variable drag coefficient proposed by Zhu et al. (2005) (see Eq. A.14), noting that there is no drag force for small immersion depths $h/R \leq 0.351$. The formulation is valid for low Reynolds number ($R_e \approx 10^5$). When the strip is fully immersed, R_e can be much higher at full scale. The flow can become turbulent with a significant effect on C_D. For very large penetration depths ($h/R > 10$), C_D tends to 1.2. (see Sarpkaya, 1966). In the present study, C_D is set to 1.2 for $h > 4R$.

2.4. Final expression of the horizontal force

The total distributed load as a function of the penetration depth with respect to the free surface is:

$$dF_{tot}(h) = \left(\rho A(h)\frac{dU}{dt} + m_a\frac{dU}{dt} + \frac{dm_a}{dh}U^2 + m_a UW_{,z} + \rho C_D(h)RU|U|\right)dl \tag{5}$$

For large h ($h > 4R$), the added mass does not vary any longer. Thus $\frac{dm_a}{dh} = 0$ and $m_a = 1$. The load formulation reduces to the Morison FNL model with constant coefficients $C_m = 2$ and $C_D = 1.2$. Since this model is based on the Generalized von Kármán Model, is it referred to as "GvKM" hereafter.

2.5. 2D Linearized Wagner Model

In order to improve predictions in the early stages of the breaking wave impact, the second model is based on Wagner's theory for the first instants of penetration in the fluid. The LWM provides the time variation of the expanding wetted surface.

In Wagner's theory, the fluid is incompressible and the flow is irrotational and inviscid (potential theory). Gravity and surface tension effects are neglected. Here we consider that the body enters a flat free surface with a vertical velocity U. The penetration depth, $h(t)$, is supposed to be small compared to the dimensions of the wetted surface. Under these assumptions, the problem is linearized, yielding the so-called flat-disk approximation (see Fig. 2).

The geometry of the half circle is defined by,

$$x = f(y) = R - \sqrt{R^2 - y^2}, y \in [0,R] \tag{6}$$

The Wagner condition (Korobkin, 1996) applied to a 2D circular cylinder yields

$$E(c/R) = \frac{\pi}{2}(1 - h/R) \tag{7}$$

with E the complete elliptic integral function of the second kind (Gradshteyn and Ryzhik, 1994, formulae 8.112, p. 860). $c(t)$ is the half-length of the wetted length. The configuration is symmetrical with respect to the axis $y = 0$.

2.6. Pressure distribution

The pressure distribution is approximated by using the MLM (Korobkin, 2004). The MLM pressure is formulated as follows:

$$P(y,t) = \rho\dot{h}^2\left[\frac{\dot{c}}{h}.\frac{c}{\sqrt{c^2-y^2}} - \frac{1}{2}.\frac{c^2}{c^2-y^2}.\frac{1}{1+f_{,y}^2} - \frac{1}{2}.\frac{f_{,y}^2}{1+f_{,y}^2}\right] + \rho\ddot{h}\left[(f-h) + \sqrt{c^2-y^2}\right] = P_v(y,t) + P_a(y,t) \quad (8)$$

As suggested in Korobkin et al. (2014), the force decomposition is possible by integrating P_v only where $P_v > 0$. This is done presently. Special attention is paid to the discretization of the body when integrating P_v in the vicinity of the contact point, where a pressure peak appears and then vanishes abruptly.

The force resulting from the integration of the pressure given by the MLM can then be written (Korobkin et al., 2014):

$$F_{MLM} = \dot{h}^2 F_v(h) + \ddot{h} F_a(h) \quad (9)$$

with

$$F_v(h) = 2\int_0^{c^*} P_v(y,t)dy \quad (10)$$

with c^* verifying $P_v(c^*,t) = 0$, and

$$F_a(h) = \rho\left[\frac{\pi}{2}c^2 - 2hc + 2\int_0^c f(y)dy\right] \quad (11)$$

Eq. 9 is of the same form as the time-rate of change of momemtum (see Eq. 1). $F_a(h)$ can then be interpreted as the added mass of the body. At the first instants of penetration, the terms F_a and F_v substitute m_a and $\frac{dm_a}{dh}$ in Eq. 5.

2.7. Continuity of the added mass without flow separation

To keep the inertia hydrodynamic load continuous with h, a transition between the added mass predicted by the MLM and the added mass predicted by the GvKM is defined. The MLM is used up to the penetration depth for which flow separation is expected. The method for computing this penetration depth relies on the FBC model (Tassin et al., 2014) and is described hereafter.

The FBC model extends the validity of the LWM for large penetration depths. A fictitious body is added to the real body so that the Wagner condition (Korobkin, 1996) can be applied to both shapes. In the circular cylinder's case, Tassin et al. (2014) suggest using a line tangent to the cylinder. The angle α (see Fig. 3) between the fictitious line and the horizontal axis needs to be defined. With $\alpha = 60°$, the results with the FBC method show the best agreement with the experiments from Campbell and Weynberg (1980) for large penetration depths (see Fig. 9 in Tassin et al., 2014).

Here, we seek to determine the penetration depth for which the flow separates. From the tangency condition of the fictitious line on the real body, the wetted correction for which there is flow separation defines the beginning of the transition. The wetted correction of transition c_{trans} is introduced

$$c_{trans} = \frac{R\tan(\alpha)}{\sqrt{1+\tan(\alpha)^2}} \quad (12)$$

Substituting (12) in (7), the penetration depth of transition h_{trans} is obtained

$$\frac{h_{trans}}{R} = 1 - 2\frac{E\left(\frac{c_{trans}}{R}\right)}{\pi} \quad (13)$$

With $\alpha = 60°$; $h_{trans}/R \simeq 0.23$.

The added mass is computed using Eq. 11. For $h_{trans}/R = 0.23$, $F'_a = \frac{F_a}{\rho\pi R^2} = 0.33$. The added mass should be continuous during the immersion. A linear interpolation between the added mass predicted by the MLM and the added mass predicted by the GvKM is proposed. The interpolation is defined from $h_{trans}/R = 0.23$ to $h/R = 1$, so as to have a smooth transition. For a circular cylinder close to a free surface, $C_a = \frac{m_a}{\rho\pi R^2} = 0.5$ for $h/R = 1$. F'_a is defined by

$$F'_a(\frac{h}{R}) = a\frac{h}{R} + b \text{ , for } \frac{h}{R} \in [0.23,1] \tag{14}$$

with $a = 0.22$ and $b = 0.28$.

From h_{trans}, we also define F_v such that $F'_v(h) = \frac{F_v}{\rho\pi R} = \frac{dF'_a(h)}{dh}$, so as to have the time-rate of change of fluid momentum $\frac{d(F_a\dot{h})}{dt} = \dot{h}^2 F_v(h) + \ddot{h}F_a(h)$. For $\frac{h}{R} \in [0.23,1]$, $F'_v(h) = 0.22$. For penetration depth $h/R \geq 1$, the added mass presented in Greenhow and Ahn (1988) is used. Fig. 4 illustrates the relative position of the cylinder with respect to the free surface. Since the model presently described combines Wagner's theory by using the MLM for the early stages of immersion and then von Kármán's theory, it is referred to as CWvKM (Composite Wagner-von Kármán Model) hereafter. Fig. 5 shows the comparison between the added mass predicted by the GvKM and its derivative with respect to the penetration depth, and the proposed formulation CWvKM. Since the wetted surface is larger in the frame of Wagner's theory than in von Kármán's theory, so the added mass is larger as well.

Fig. 6 sums up the variation of the different quantities and coefficients involved in the computation of the hydrodynamic load $dF_{tot}(h)$ with the CWvKM.

- For $h < h_{trans}$; F_a and F_v are computed from the numerical integration of MLM (Eq. 8) on the wetted surface predicted by the LWM.
- For $h_{trans} \leq h < R$; the total load is computed with equation (5) by using the linear transition defined by Eq. 14.
- For $R \leq h$; F_a is equal to the added mass predicted by the GvKM and $F_v = \frac{dm_a}{dh}$.

2.8. Strip theory approach

The cylinder is divided into strips ($\frac{dl}{R} = 0.01$) which are the support of integration of the forces in the semi-analytical models. The shape and kinematics of the wave interacting with the cylinder are a necessary input for the semi-analytical models and are derived from 2D CFD simulations of focused breaking wave packets (Batlle et al., 2022) for the present study. At each instant, the intersection of the cylinder with respect to the undisturbed free surface is used to compute the penetration depth of each strip. The models include different stages depending on the immersion, and the kinematics varies greatly in the crest. Fluid velocity is then post-processed vertically in the fluid domain at the cylinder axis x_{axis} and $x_{axis} \pm R$, as well as at the free surface. We consider the average kinematics along the length of the strip, assuming that the kinematics varies linearly between the water columns and the free surface. For example, if $h < R$, the average horizontal velocity on the strip at z is $U(z) = \frac{U_{x_{axis}-R}(z) + U_{x_{axis}-R+h}(z)}{2}$, with $U_{x_{axis}-R}$ the horizontal velocity at $x_{axis} - R$ and $U_{x_{axis}-R+h}$ the horizontal velocity at the free surface.

3. Comparison of the models

The developed semi-analytical models are compared to different existing impact load models by the example focused breaking wave impact on a circular cylinder. Three different constant steepness wave packets are considered, labelled A3, A4, A6, following Derakhti et al. (2018). These have global wave steepnesses $S = \sum_{n=1}^{N} a_n k_n$ of 0.302, 0.31, and 0.44, using $N = 32$ spectral components, uniformly distributed between 0.55 Hz and 1.21 Hz (central

frequency 0.88 Hz), in a depth of 0.60 m (Derakhti et al., 2018). a_n and k_n are respectively the amplitude and the wavenumber of the n^{th} frequency component. The shape and kinematics of the waves as a necessary input to the load models were computed by 2D simulations with the open-source CFD software code_saturne developed by EDF R&D. The same solver was used for full 3D simulations with a cylinder, which will serve for further comparison in the following. Further details about the numerical simulations can be found in Batlle et al. (2022). In order to have a size similar to those that will be deployed in the DIMPACT project basin tests, a bottom-fixed cylinder of radius R = 0.1 m is located at the breaking location in the 3D simulations. The 2D waves and the cylinder in the wave field are presented in Fig. 7. The case referred to as "A6 nearly breaking wave" corresponds to case A6 with the cylinder located 0.2 m upstream.

The cylinder is divided into four sections of thickness $\frac{H}{R} = 0.9$ (see Fig. 7). Sections are referenced from 1 to 4 from top to bottom. For each case, the force is computed in the 4 sections of the segmented cylinder. Comparisons are made between 5 formulations: CWvKM, GvKM, the CFD results and load formulations inspired by the two models presented in Nestegård et al. (2004); Hansen and Kofoed-Hansen (2017). The first formulation (Nestegård et al., 2004) uses Campbell & Weynberg formula (referred to as "C&W") (Eq. A.6) and the second (Hansen and Kofoed-Hansen, 2017) uses Goda formula (Eq. A.5) for the partially submerged strips. When the strip is fully immersed, the hydrodynamic load is computed using Morison equation (referred to as "M") with constant coefficients (C_m = 2 & C_D = 1.2). The input to those models in terms of shape and kinematics of the waves was also derived from the 2D CFD simulations, while in the original formulations from Nestegård et al. (2004) and Hansen and Kofoed-Hansen (2017) the kinematics was either estimated or extrapolated.

Then, comparisons of the total load acting on the cylinder are made between the present formulations, CFD results and the following 4 semi-analytical/empirical slamming load models: Goda (Eq. A.5), Wienke & Oumeraci (referred to as "W&O") (Eq. A.7), Paulsen (Eq. A.10), and the formulation proposed in the Wifi JIP Project (referred to as "WJP") (Eq. A.12). The impact load is estimated using a curling factor λ set to 0.4 which is a standard value (Goda et al., 1966; Wienke and Oumeraci, 2005; Lackner et al., 2018). The slamming contribution is added to the quasi-static load, computed with the CWvKM up to $z = (1 - \lambda)\eta_b$ with η_b the crest elevation. This is equivalent to using the Morison FNL model for the deeply submerged strips. In addition, the Rainey model (see Eq. A.2, A.3, A.4) is implemented with constant coefficients (C_a = 1 and C_D = 1.2).

3.1. Case A4

In Fig. 8, the time history of the load acting on each of the four sections, computed with CFD and the 4 semi-analytical models, is compared. The origin in time is fixed at T_{impact}, the time at which the maximum CFD force is reached. Section 4 is totally submerged when the wave passes and the penetration depth of the entire section is larger than $4R$. The hydrodynamic force of the GvKM and the CWvKM is similar to the Morison FNL formulation with constant inertia and drag coefficients. The relative error between the 5 models is less than 5% in this section.

The force predicted by the different models in section 3 is also similar. However, some strips of this section are not completely immersed in the time interval $t \in [-0.18, -0.10]$. The load models using C&W and Goda formulas predict a slightly lower effort (20%) compared to the CFD results and the present formulations. Since the fluid velocity is assumed to be constant in the partially submerged strips, a part of the inertia load is omitted.

Section 2 is completely dry at the beginning of the simulation and the progressive increase of the load can be observed. The load formulations inspired from Nestegård et al. (2004) (C&W + M) and Hansen and Kofoed-Hansen (2017) (Goda + M) capture a lower force (about 40% lower than the other three models). The reason is that both models consider a constant fluid velocity during the progressive immersion of the strip. Consequently, there is no effect of inertia. These effects are taken into account in the CWvKM and GvKM. The proposed models predict almost the same load in section 2. Accounting for the wetted correction by using Wagner's theory has little influence on the load acting on this section.

Finally, the force in section 1 is significantly higher using the Froude-Krylov-based approaches. As the CWvKM is based on Wagner's theory and the MLM at the first instants of penetration, the slamming coefficient is larger than the one predicted by the GvKM ($C_s = 2\pi$ for a circular cylinder impacting a flat free surface within Wagner's theory while $C_s = \pi$ within von Kármán's theory). Also, the load decay is faster for the CWvKM. This is due to the more rapid decrease of the term F_v at the first instants of penetration when considering the force from the integration of the MLM (see Fig. 5). This term is the main contribution to the slamming load since $F_v(0) \neq 0$ and $F_a(0) = 0$.

Fig. 9 shows the comparison of the total load acting on the four sections computed with the engineering formulas from Goda, W&O, WJP and Rainey. When the crest hits the structure, the impact load predicted by the semi-analytical models is much larger than the numerical results. The same observations are made in Lackner et al. (2018). Accounting for an uniform phase speed on the impact height instead of the actual fluid velocity at the free surface could lead to a highly conservative slamming load, as using W&O formulation. The slamming expression proposed by Paulsen et al. (2019) is based on Wagner's theory as well. Nevertheless, the formula incorporates the coefficient $2/\pi^2$ which is derived from the force distribution on the impact area. Therefore, the maximum load is much less conservative than with W&O formulation. Furthermore, in the formula from Goda et al. (1966) and Wienke and Oumeraci (2005) the wavefront is assumed to be vertical. This is why the maximum load is reached instantaneously and leads to an inconsistent force impulse. In the expression proposed by Paulsen et al. (2019), the load temporal development is defined from measurements. The time variation of the slamming load is quite consistent and in line with the strip-theory approaches. Formula from Goda et al. (1966), Wienke and Oumeraci (2005) and Paulsen et al. (2019) rely on the curling factor, which depends on the free surface shape. This parameter has to be user-calibrated. It increases the uncertainty of the load calculation as there is no specific criterion to estimate it.

The total load acting on the four sections of the cylinder computed with the Rainey model is slightly underestimated ($\approx$ 20%) before the impact compared to the CFD, GvKM and CWvKM. The load in the partially immersed sections (in particular section 2) is not negligible. The Rainey model accounts for this contribution with the term F_η (see Eq. A.4) which depends on $\eta_{,x}$. It is the same as considering the intersection between the wave and the cylinder as a straight line, which poorly describes the actual shape of the intersection. In particular, as the wave approaches the breaking point, the slope in front of the cylinder is much larger than behind the cylinder.

To assess the discrepancy between the CFD and the formulas based on the Froude-Krylov approach, the 2D free surface and the projection of the 3D free surface on the vertical plane (x,z) are compared in Fig. 10 at two different instants before the impact. The vertical front present on the 2D wave is flattened by the run-up and the crest is highly distorted. The 3D impact is then much softer than the 2D configuration since the vertical front disappears. This explains why the load predicted by the semi-analytical models is much higher than the CFD force. The attenuation of the impact load by the run-up has also been noticed in Ha et al. (2020); Lackner et al. (2018). Omitting the effect of the run-up in the Froude-Krylov assumption or by considering a vertical wavefront is very conservative in that case. Furthermore, the size of the structure can directly affect the run-up amplitude. A smaller ratio D/H_b, H_b being the breaking wave height, may lead to a less disturbed breaking wave.

Comparisons of the results on the other 3 waves (A3, A6 and A6 - nearly breaking wave) lead to the same general observations:

- The force acting on the completely submerged section 4 is similar for all the 5 models compared ($\approx$ 7% of maximum relative difference).
- A portion of section 3 is partially immersed at the beginning of the simulation. For $t - T_{impact} < -0.06\,s$, the models using C&W and Goda formulas predict a lower effort (between 20% and 30%) than the CFD and the two proposed immersion models.
- The load in section 2 predicted by the CFD, GvKM and CWvKM are quite similar. The models inspired from Nestegård et al. (2004); Hansen and Kofoed-Hansen (2017) (C&W + M and Goda + M) lead to a 40-60% lower effort compared to the other three models. Fig. 11 shows the comparison of the load acting on section 2 for the other three cases.
- The force in section 1 is much higher by using the Froude-Krylov approaches. Indeed, the comparison of 2D and 3D free surfaces show that the 3D crest is flattened. The wavefront is much less steep, which dampens the impact load compared to the 2D cases.

3.2. Comparison of the total load induced by the four waves

Fig. 12 shows the total load acting on the 4 sections of the cylinder for the different cases.

Case A3 is a weak-spilling breaking wave. This wave induces the smallest effort on the cylinder and is the less violent wave. Although the wave impacts the structure, the force peak is not present in the CFD results. This is because of the flattening of the wavefront by the cylinder. The total load predicted by the semi-analytical models

deviates from the CFD effort, especially because the force in section 2 is slightly larger compared to the numerical results (see Fig. 11). This trend can be seen in the case A4 too. Case A4 is a spilling breaking wave and has the same height as case A3. This wave induces a 20% higher effort than case A3.

Case A6 is a plunging breaking wave with a height 17% higher than cases A3 and A4. The total force acting on the structure is much greater: 106% and 76% larger than A3 and A4 respectively. The sudden rise in force, characteristic of wave impact loads, is clearly identifiable.

Lastly, case A6 - nearly breaking wave, also induces greater efforts than A3 and A4 while the wave is not yet breaking. Visually, the wave is much more violent and the front is steeper than in cases A3 and A4 (see Fig. 7). The quasi-static load, before the impact, is similar between the CFD and the present formulations for the last two cases. The total load is larger with the semi-analytical formulas since the crest is distorted when the wave approaches the structure.

4. Discussion

Fig. 13 shows the force distribution dF_{tot} at the instant of maximum load for case A4. The force distribution is discontinuous when the load model is abruptly changed at $h = D$. This is clearly visible between $z/\eta = 0.2$ and $z/\eta = 0.6$ in Fig. 13. The contribution of section 2 to the total load is equivalent to that of section 3 and therefore needs to be accurately predicted. For instance, to compute the overturning moment, the force distribution is integrated along the cylinder so it is important to capture the load on each strip accurately. Our models, accounting for fluid acceleration and omitting flow separation, predict a similar load to the CFD in the partially immersed strips.

Between $z/\eta = 0.1$ and $z/\eta = 0.7$, the force distribution presents some irregularities. Indeed, U (see Fig. 14) and W (see Fig. 15) are discontinuous in this portion. Because of the Volume of Fluid method implemented in the Navier-Stokes solver (Batlle et al., 2022), the velocity components are not smooth when getting close to the free surface. A finer mesh at the interface air/water could solve this issue.

The main differences in terms of load between the CFD and the semi-analytical models are in section 1, where the impact occurs. A comparison between the 2D free surface and the 3D wave shape shows that the crest is highly distorted. The run-up flattens the crest, which no longer has a vertical front. With the CFD, the slamming is much softer in 3D than in 2D disregarding the presence of the structure.

Engineering formulas from Goda et al. (1966); Wienke and Oumeraci (2005) and from the Wifi JIP Project predict only the maximum load and possibly its decay. Expression from Paulsen et al. (2019), which includes empirical corrections, gives a generic formula with a reasonable time variation and an estimate of the total load. In the experiments of Wienke and Oumeraci (2005); Ridder et al. (2017); Paulsen et al. (2019), the ratio D/H_b was significantly lower than for the waves hereby presented. Their formulations might be more suitable for a low ratio D/H_b. However, in Lackner et al. (2018), this ratio is similar to that found in Wienke and Oumeraci (2005); Paulsen et al. (2019) and the conservative nature of the Goda and W&O formulations is emphasized as well.

The models presented in this paper capture the quasi-static load and the slamming contribution without any assumptions about the wave. Furthermore, since the CWvKM is based on the MLM at the early stages of immersion, the pressure distribution on the impact area of the cylinder is provided. There are no special user-adjusted parameters, such as the curling factor, or empirical corrections, such as in Paulsen formula.

5. Conclusion

Two semi-analytical models are considered for estimating the hydrodynamic load of breaking waves impacting a fixed rigid vertical cylinder. The present approaches are based on considering the rate of change of momentum and enforcing continuity of the added mass during the penetration of a cylinder in the fluid. The first model accounts for the real shape of the body through the Generalized von Kármán Model (GvKM). The nonlinearity of the flow kinematics is taken into account in the inertia load by considering the quadratic terms of the momentum equation. The total load is obtained by adding the drag force. A second model based on Wagner's theory, and the MLM approach is presented to account for the pile-up effect at the first instants of penetration. In the CWvKM, the added mass remains continuous by linearly interpolating the added mass predicted by the integration of the MLM and the added mass predicted by the GvKM. Here, diffraction effects are omitted. The fully nonlinear kinematics of an undisturbed phase-focused breaking wave is accounted for in a strip-wise manner.

The loads in the different sections of the segmented cylinder and the total force are compared between 3D numerical results including a fixed vertical cylinder, the present models and other formulations. Since the wave crest is greatly deformed by the cylinder, the force predicted using the Froude-Krylov hypothesis is much larger in the highest section than the CFD results. The wave loads in the lower sections are similar between the different models. In the partially submerged sections, the numerical results and the proposed semi-analytical models are very close, while the formulations inspired by the models presented by Nestegård et al. (2004); Hansen and Kofoed-Hansen (2017) predict a much smaller force. From a practical point of view, the GvKM model can be easily implemented to compute the extreme wave forces in the strips under the impacting part of the wave.

In future works, as part of the DIMPACT project, focused waves will be generated in the experimental facility of Ifremer (Brest), and the semi-analytical models and CFD results will be compared to the experimental data. More severe breaking waves will be considered, in particular strong plunging breakers, whose crests may be less deformed by the presence of the cylinder, but where flow separation may be expected. By knowing the height over which the flow separates, Wagner's theory and the FBC model can be applied directly instead of considering a growing added mass.

Declaration of competing interest

The authors declare that they have no known competing financial interests or personal relationships that could have appeared to influence the work reported in this paper.

Acknowledgments

This work is performed under financial support of grant ANR-10-IEED-0006-34, France Energies Marines project DIMPACT (Design of FOWT and IMPACTs of energetic steep and breaking waves).

6. CRediT author statement

Paul Renaud: Methodology, Conceptualization, Software, Writing - Original Draft, Writing - Review & Editing. **Marc Batlle Martin**: Methodology, Software, Writing - Original Draft, Writing - Review & Editing. **Florian Hulin**: Writing - Review & Editing. **Jeffrey C. Harris**: Methodology, Software, Writing - Review & Editing, Supervision. **Yves-Marie Scolan**: Methodology, Conceptualization, Writing - Review & Editing, Supervision. **Jean-François Filipot** : Conceptualization, Project administration, Funding acquisition, Writing - Review & Editing, Supervision.

References

Y. Goda, S. Haranaka, M. Kitahata, Study of impulsive breaking wave forces on piles, Report of Port and Harbor Research Institutes 5 (1966) 1–30.

J. Wienke, H. Oumeraci, Breaking wave impact force on a vertical and inclined slender pile - theoretical and large-scale model investigations, Coastal Engineering 52 (2005) 435–462.

M. Alagan Chella, A. Tørum, D. Myrhaug, An overview of wave impact forces on offshore wind turbine substructures, Energy Procedia 20 (2012) 217–227.

B. Paulsen, B. Sonneville, M. van der Meulen, N. Jacobsen, Probability of wave slamming and the magnitude of slamming loads on offshore wind turbine foundations, Coastal Engineering 143 (2019) 76–95.

A. Nestegård, K. Hagatun, S. Haver, A. Kalleklev, Y. Wu, E. Lehn, Resonant vibrations of riser guide tubes due to wave impact, in: 23rd International Conference on Offshore Mechanics and Arctic Engineering, 2004.

H. F. Hansen, H. Kofoed-Hansen, An engineering-model for extreme wave-induced loads on monopile foundations, in: ASME 2017 36th International Conference on Ocean, Offshore and Arctic Engineering, American Society of Mechanical Engineers Digital Collection, 2017.

J. Morison, J. Johnson, S. Schaaf, The force exerted by surface waves on piles, J Petrol Technol 2 (1950) 149–154.

H. Bredmose, et al., Derisk — accurate prediction of uls wave loads. Outlook and first results, Energy Procedia 94 (2016) 379–387.

L. Suja-Thauvin, E. Bachynski, F. Pierella, M. Borg, J. Krokstad, H. Bredmose, Critical assessment of hydrodynamic load models for a monopile structure in finite water depth, Marines Structures 72 (2020).

W. Manners, R. Rainey, Hydrodynamic forces on fixed submerged cylinders, in: Proc Roy Soc Lond A Jan. 1992;436(1896):13–32., 1992.

F. Pierella, A. Ghadirian, H. Bredmose, Extreme wave loads on monopile substructures: precomputed kinematics coupled with the pressure impulse slamming load model, in: Proceedings of International Offshore Wind Technical Conference 2019 American Society of Mechanical Engineers, 2019.

R. Rainey, A new equation for calculating wave loads on offshore structures, J. Fluid Mech 204 (1989) 295–324.
M. A. El-Reedy, Chapter 7 - assessment of existing structures and repairs, in: M. A. El-Reedy (Ed.), Offshore Structures, Gulf Professional Publishing, Boston, 2012, pp. 445–561.
X. Zhu, O. Faltinsen, C. Hu, Water entry and exit of a horizontal circular cylinder, Journal of Offshore Mechanics and Arctic Engineering 129 (2005).
T. Sarpkaya, Separated flow about lifting bodies and impulsive flow about cylinders, AIAA J 44 (1966) 414–420.
C. Clément, P. Bozonnet, G. Vinay, P. Pagnier, B. Nabal Borras, J. Réveillon, Evaluation of Morison approach with CFD modelling on a surface-piercing cylinder towards the investigation of FOWT hydrodynamics, Ocean Engineering 251 (2022).
T. von Kármán, The Impact of Seaplane Floats during Landing, Technical Report, Technical Note 321, NACA, 1929.
H. Wagner, Über Stoss- und Gleitvorgange an der Oberfläche von Flüssigkeiten, Zeitschrift fur Angewandte Mathematik und Mechanik 12 (1932) 193–215.
S. Malenica, A. Korobkin, Some aspects of slamming calculations in seakeeping, 9th International Conference on Numerical Ship Hydrodynamics (2007).
R. Zhao, O. Faltinsen, J. Aarsnes, Water entry of arbitrary two-dimensional sections with and without separation, in: The 21st Symposium on Naval Hydrodynamics. Trondheim, Norway., 1996.
I. Campbell, P. Weynberg, Measurement of parameters affecting slamming, Technical Report, University of Southampton : Wolfson Unit for Marine Technology, 1980.
R. Cointe, J.-L. Armand, Hydrodynamic impact analysis of a cylinder, J Offshore Mech Arctic Eng 109 (1987) 237–243.
A. Korobkin, Analytical models of water impact, Euro. Jnl of Applied Mathematics 15 (2004) 821–838.
A. Tassin, N. Jacques, A. El Makli Alaoui, A. Nême, B. Leblé, Assessment and comparison of several analytical models of water impact, Int. Jnl. of Multiphysics 4 (2010).
A. Tassin, D. Piro, A. Korobkin, K. Maki, M. Cooker, Two-dimensional water entry and exit of a body whose shape varies in time, Journal of Fluids and Structures (2013) 317–336.
A. Korobkin, T. Khabakhpasheva, S. Malenica, Y. Kim, A comparison study of water impact and water exit models, Int. J. Nav. Archit. Ocean Eng. 6 (2014) 1182–1196.
Z. Sun, X.-p. Sui, A. Korobkin, L. Zou, Z. Zong, Slamming force decomposition with gravity effect, Journal of Fluids and Structures (2022) 1182–1196.
A. Tassin, A. Korobkin, M. Cooker, On analytical models of vertical water entry of a symmetric body with separation and cavity initiation, Applied Ocean Research 48 (2014) 33–41.
R. Hascoët, N. Jacques, Y.-M. Scolan, A. Tassin, A two-dimensional analytical model of vertical water entry for asymmetric bodies with flow separation, Applied Ocean Research 92 (2019).
E. J. Ridder, T. Bunnik, J. M. Peering, B. T. Paulsen, C. Wehmeyer, P. Gujer, E. Asp, Summary of the Joint Industry Project Wave Impact on Fixed Foundations (WIFI JIP), in: Proceedings of the ASME 2017 36th International Conference on Ocean, Offshore and Arctic Engineering, OMAE 2017, Trondheim, Norway, 2017.
DNV, Recommanded practice. DNV-RP-C205. Environmental Conditions and Environmental Loads, 2021.
R. McCamy, R. Fuchs, Wave forces on piles, a diffraction theory, Technical Report, U.S. Army Corps of Engineers, Beach Erosion Board, 1954.
P. Kaplan, M. Silbert, Impact forces on platform horizontal members in the splash zone, in: Proceedings of Offshore Technology Conference, Houston, Texas, 1976, pp. 749–758.
T. Sarpkaya, Wave impact loads on cylinders, in: Offshore Technology Conference, Houston, 1978.
G. Khalil, M. Ali, An investigation into wave slamming loads on horizontal circular cylinders, Journal of the Institution of Engineers Malaysis 55 (1994) 19–28.
S. Prasad, Wave impact forces on a horizontal cylinder, Ph.D. thesis, University of British Columbia, 1994.
S. Akter, Hydrodynamic Analysis of wave Slamming on a Horizontal Circular Cylinder, Master's thesis, Bangladesh University of Engineering and Technology, 2011.
M. Greenhow, S. Ahn, Added mass and damping of horizontal circular cylinder sections, Ocean Engineering 15 (1988) 495–504.
M. M. Batlle, J. C. Harris, P. Renaud, F. Hulin, J.-F. Filipot, Numerical investigation of slamming loads on floating offshore wind turbines, in: Proceedings of the 32nd International Offshore and Polar Engineering Conference, Shanghai, China, 2022.
A. Korobkin, Water impact problems in ship hydrodynamics, volume 5 of *Advances in Marine Hydrodynamics*, Computational Mechanics Publications, 1996, pp. 323–371.
I. Gradshteyn, I. Ryzhik, Tables of integrals, New York Academic Press, 1994.
M. Derakhti, M. Banner, J. Kirby, Predicting the breaking strength of gravity water waves in deep and intermediate depth, J. Fluid Mech. 848 (2018).
M. Lackner, D. Schmidt, S. Arwade, A. Myers, A. Robertson, Simulating breaking waves and estimating loads on offshore wind turbines using computational fluid dynamic models, Technical Report, University of Massachusetts Amherst, 2018.
Y.-J. Ha, K.-H. Kim, N. B.W., S. Hong, Experimental investigation for characteristics of wave impact loads on a vertical cylinder in breaking waves, Ocean Engineering 209 (2020).

A. Wave load models

A.1. Quasi-static wave load models

Morison equation (Morison et al., 1950):

$$dF = \left(\rho C_m A \frac{dU}{dt} + \frac{1}{2}\rho C_D D U|U|\right) dl \tag{A.1}$$

with $C_m = 1 + C_a$.

Morison Fully Non Linear "FNL" (Suja-Thauvin et al., 2020):

$$dF = \left(\rho C_m A \frac{dU}{dt} + \rho\pi R^2 C_a U W_{,z} + \frac{1}{2}\rho C_D D U|U|\right) dl \tag{A.2}$$

with

$$\frac{dU}{dt} = U_{,t} + U U_{,x} + W U_{,z} \tag{A.3}$$

Rainey model (Morison FNL + Point force) (Rainey, 1989; Manners and Rainey, 1992):

$$F_\eta = -\frac{1}{2}\rho\pi R^2 C_a U^2 \eta_{,x} \tag{A.4}$$

η being the free surface elevation at the cylinder.

A.2. Slamming coefficients

Goda et al. (1966):

$$C_s(t) = \pi\left(1 - \frac{V}{R}t\right) \tag{A.5}$$

Campbell and Weynberg (1980):

$$C_s(h) = 5.15\left[\frac{D}{D + 19h} + \frac{0.107h}{D}\right] \tag{A.6}$$

Wienke and Oumeraci (2005), with cylinder tilt $\gamma = 0$:

$$C_s(t) = \left(2\pi - 2\sqrt{\frac{Vt}{R}}\, arctanh\sqrt{1 - \frac{Vt}{4R}}\right) \text{for } 0 \le t \le \frac{R}{8V} \tag{A.7}$$

$$C_s(t) = \left(\pi\sqrt{\frac{1}{6Vt'/R}} - \sqrt{\frac{8Vt'}{3R}}\, arctanh\sqrt{1 - \frac{Vt'}{R}\sqrt{\frac{6Vt'}{R}}}\right) \text{for } \frac{3R}{32V} \le t' \le \frac{12R}{32V} \tag{A.8}$$

with

$$t' = t - \frac{R}{32V} \tag{A.9}$$

A.3. Slamming load formulas

Paulsen et al. (2019):

$$F_s(t) = \frac{1}{2}\rho V^2 C_s f(t) \lambda H_b D g(z',y') \tag{A.10}$$

with

$$V = \sqrt{gd};\ C_s = 2\pi;\ f(t) = sin^2(\pi \frac{t}{T_{impact}});\ g(z',y') = \frac{2}{\pi^2} \tag{A.11}$$

where d is the local water depth and $T_{impact} = \frac{13D}{32V}$.

Wifi JIP Project:

$$F_s = \frac{1}{2}\rho u^2 C_s A \tag{A.12}$$

with

$$u = 1.1V;\ C_s = 2\pi;\ A = \frac{1}{32}\pi H_b D \tag{A.13}$$

V being the phase velocity.

A.4. Drag coefficient

Zhu et al. (2005):

$$C_D = p_1 h'^5 + p_2 h'^4 + p_3 h'^3 + p_4 h'^2 + p_5 h' + p_6 \tag{A.14}$$

with $h' = h/R - 0.351$. For $h' \leq 0, C_D = 0$. The coefficients p_i are given in Zhu et al. (2005).

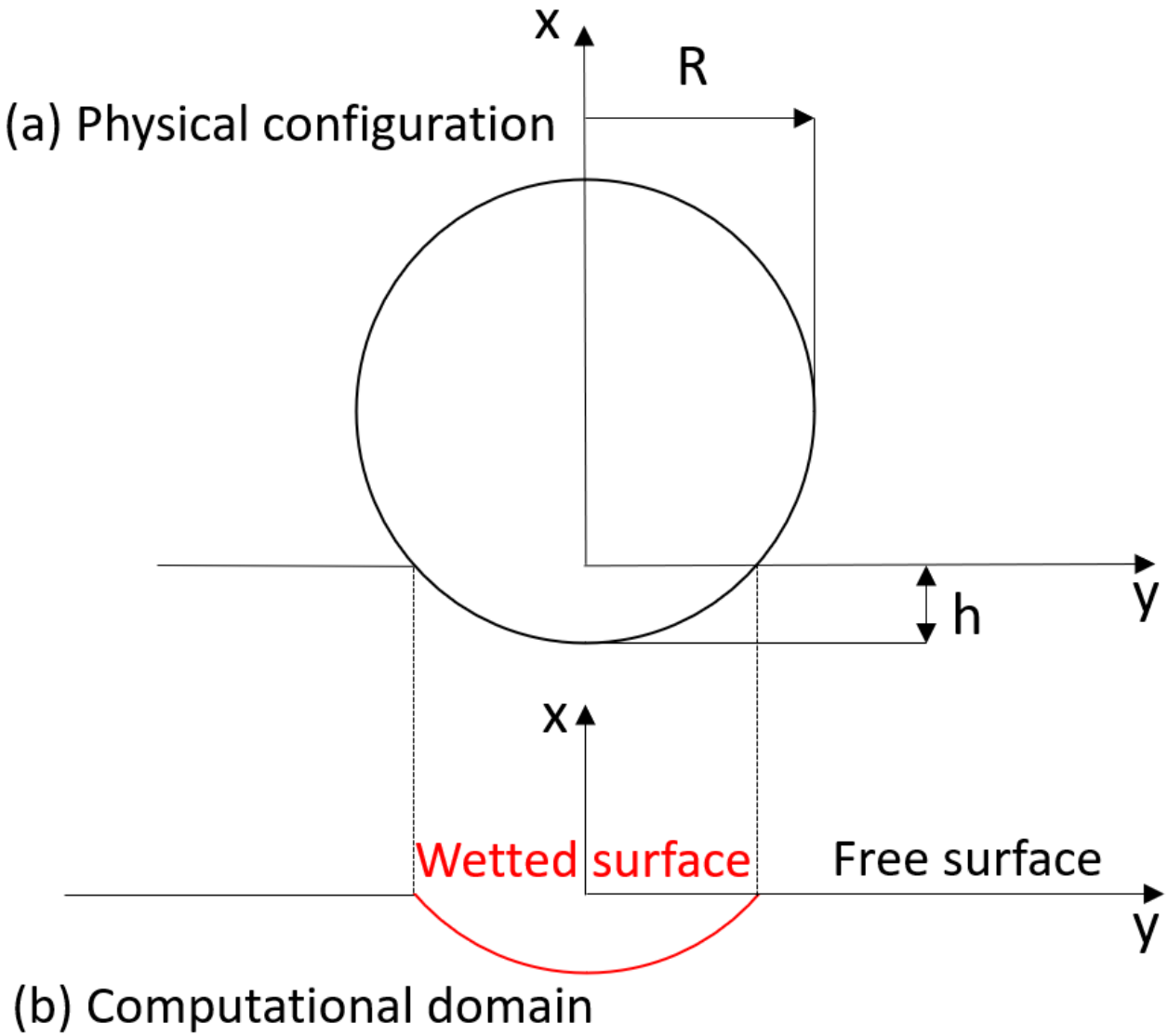

Figure 1: Sketch of the relative position of the cylinder and the free surface after impact over a penetration depth h in the framework of the GvKM.

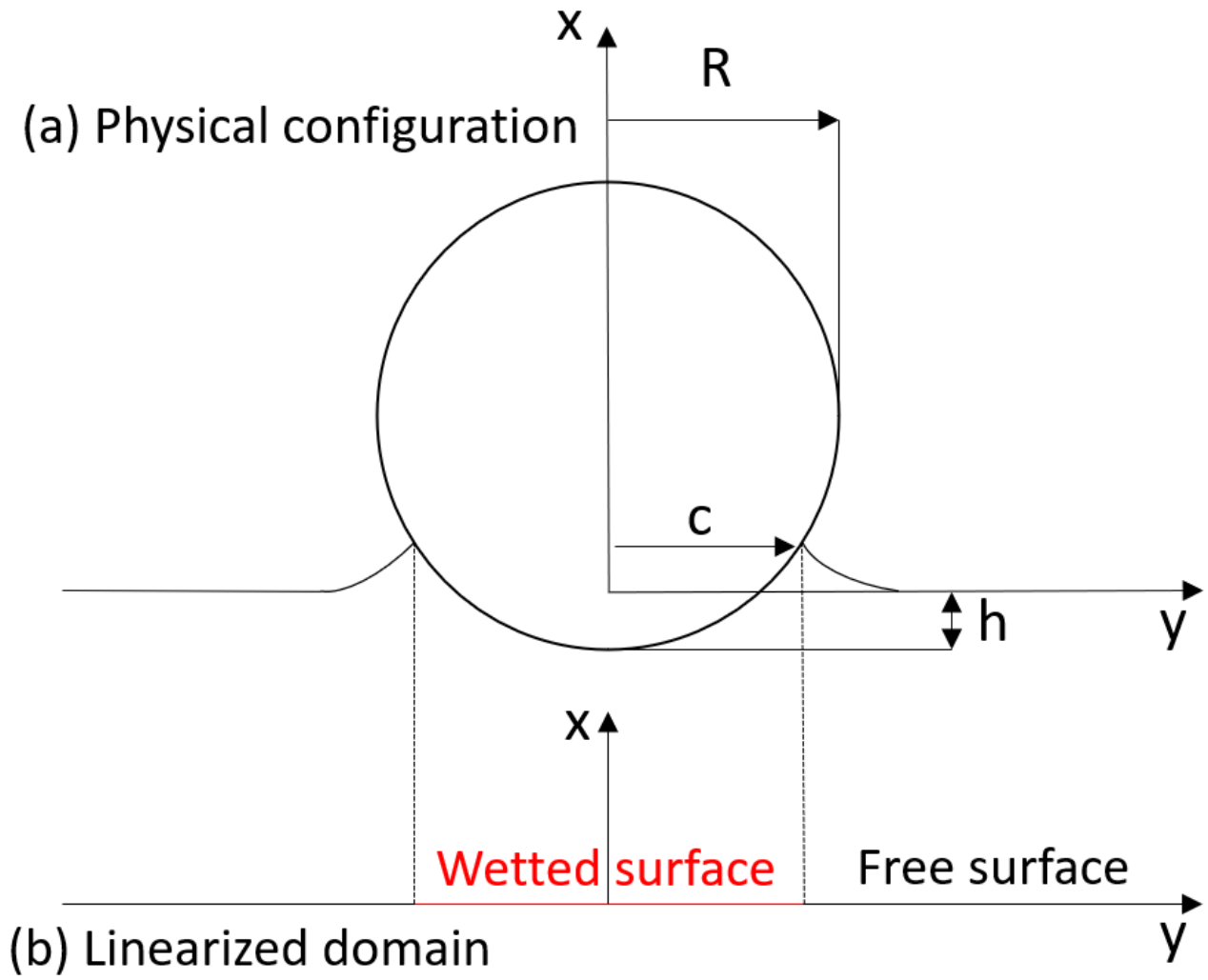

Figure 2: Sketch of the relative position of the cylinder and the free surface after impact over a penetration depth h. (a) Physical configuration, (b) Linearized domain. The jet that emanates at the contact point $|y| = c$ is not represented.

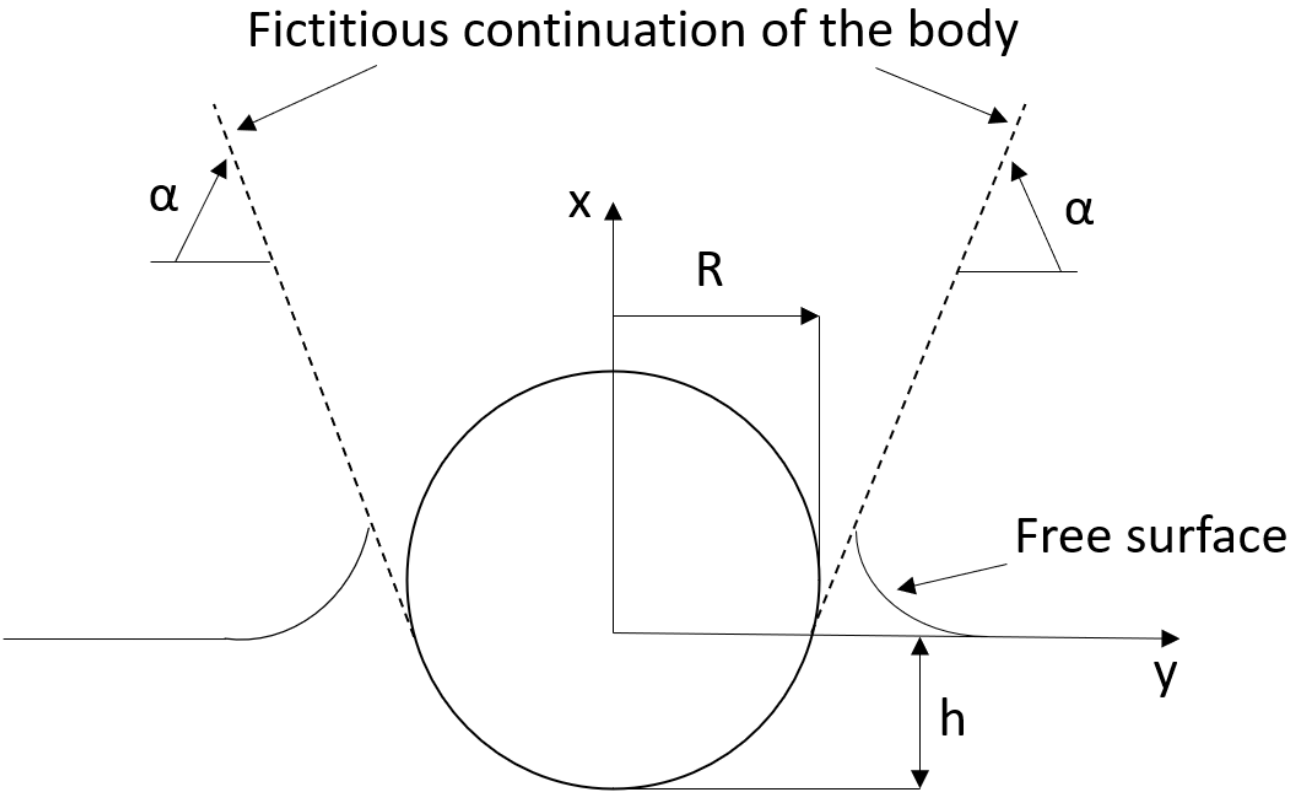

Figure 3: Illustration of the FBC concept for the vertical water entry of a horizontal cylinder.

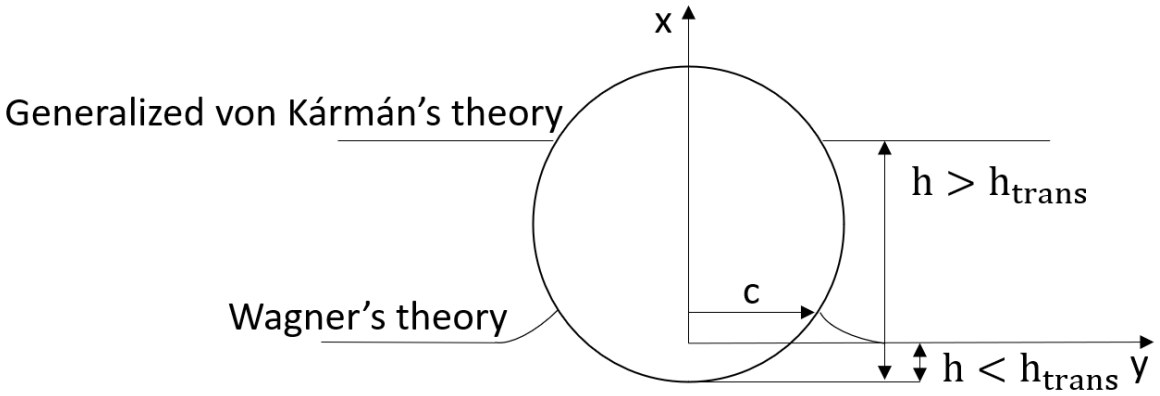

Figure 4: Sketch of the relative position of the cylinder and the free surface after impact over a penetration depth $h < h_{trans}$, considering the wetted correction (Wagner's theory), and over a penetration $h > h_{trans}$ (Generalized von Kármán's theory).

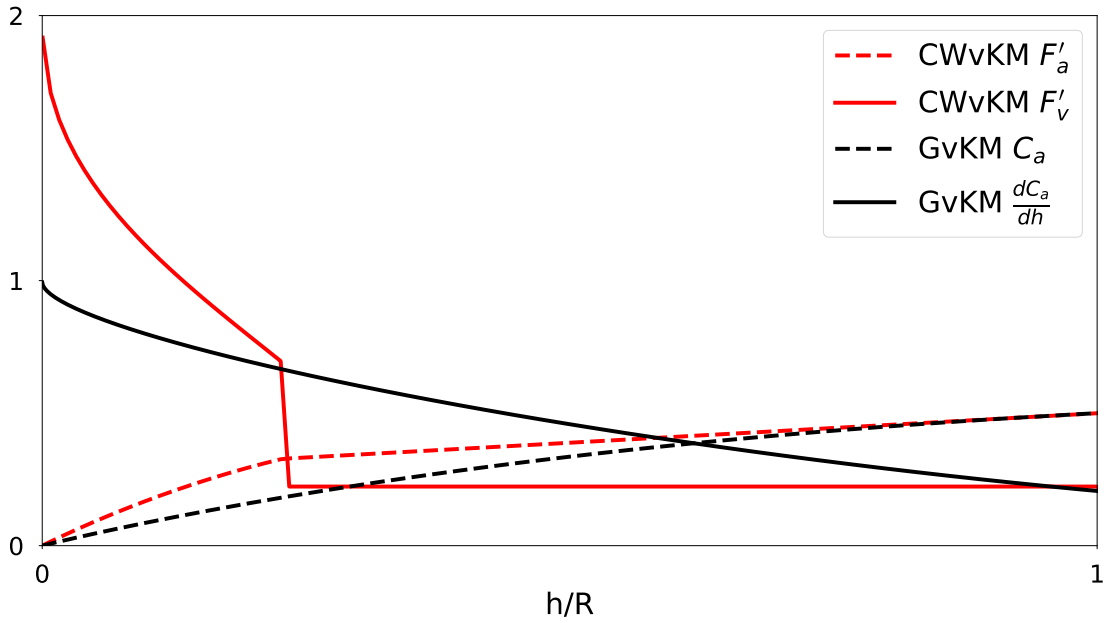

Figure 5: High frequency limit of added mass coefficient of a circular cylinder close to a free surface (GvKM C_a, black dashed line) and its derivative (GvKM $\frac{dC_a}{dh}$, black solid line), the added mass coefficient (CWvKM F'_a, red dashed line) and the slamming coefficient $F'_v = \frac{F_v}{\rho\pi R}$ (CWvKM F'_v, red solid line) presented in the CWvKM as a function of the non-dimensional penetration depth.

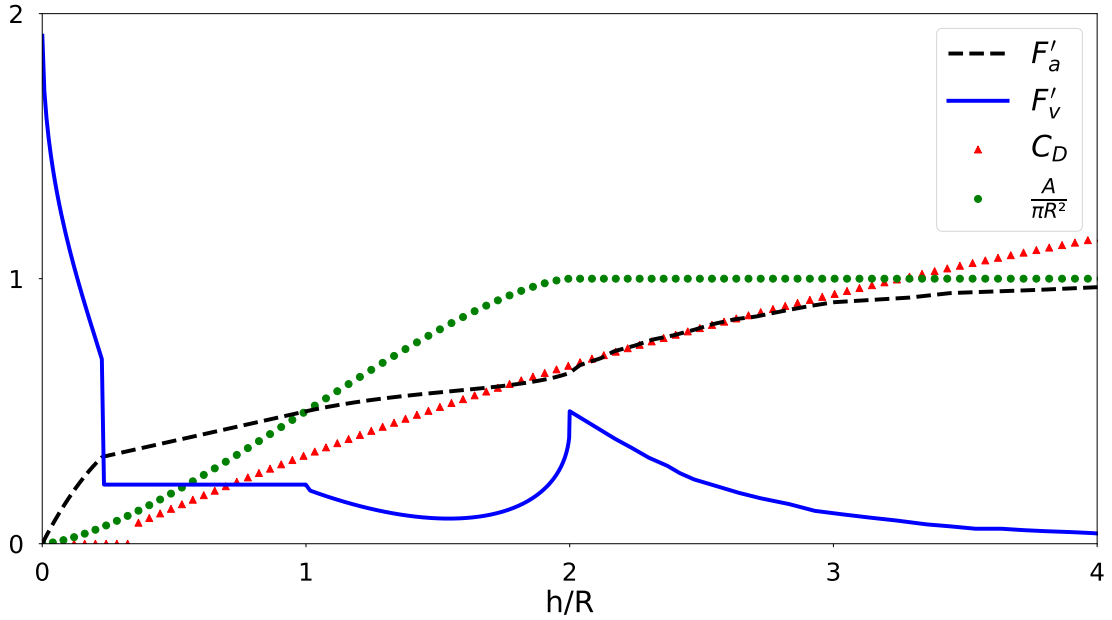

Figure 6: Variation of the different quantities during the immersion as a function of the non-dimensional penetration depth. Added mass coefficient (F'_a, dashed line), and the slamming term (F'_v, solid line) presented in the CWvKM, drag coefficient (C_D, triangle marks) and the non-dimensional immersed area ($\frac{A}{\pi R^2}$, circle marks).

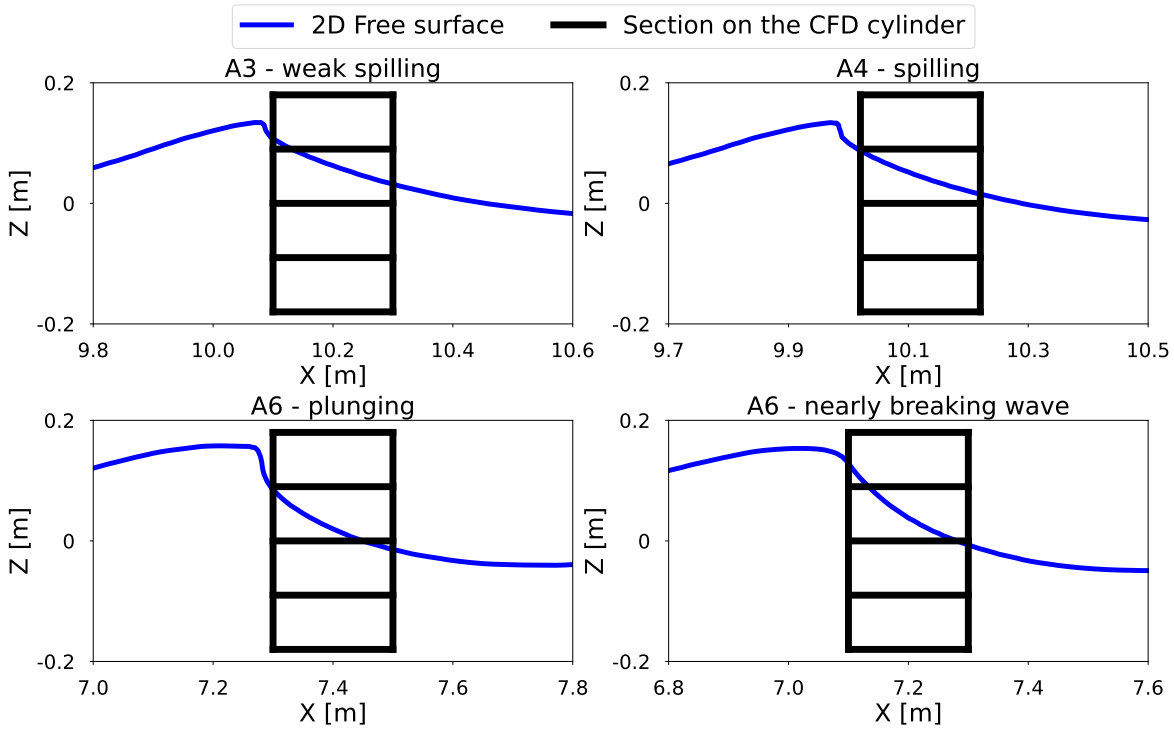

Figure 7: Free surface elevation (blue line) of the four waves, before the impact on the segmented cylinder (black line).

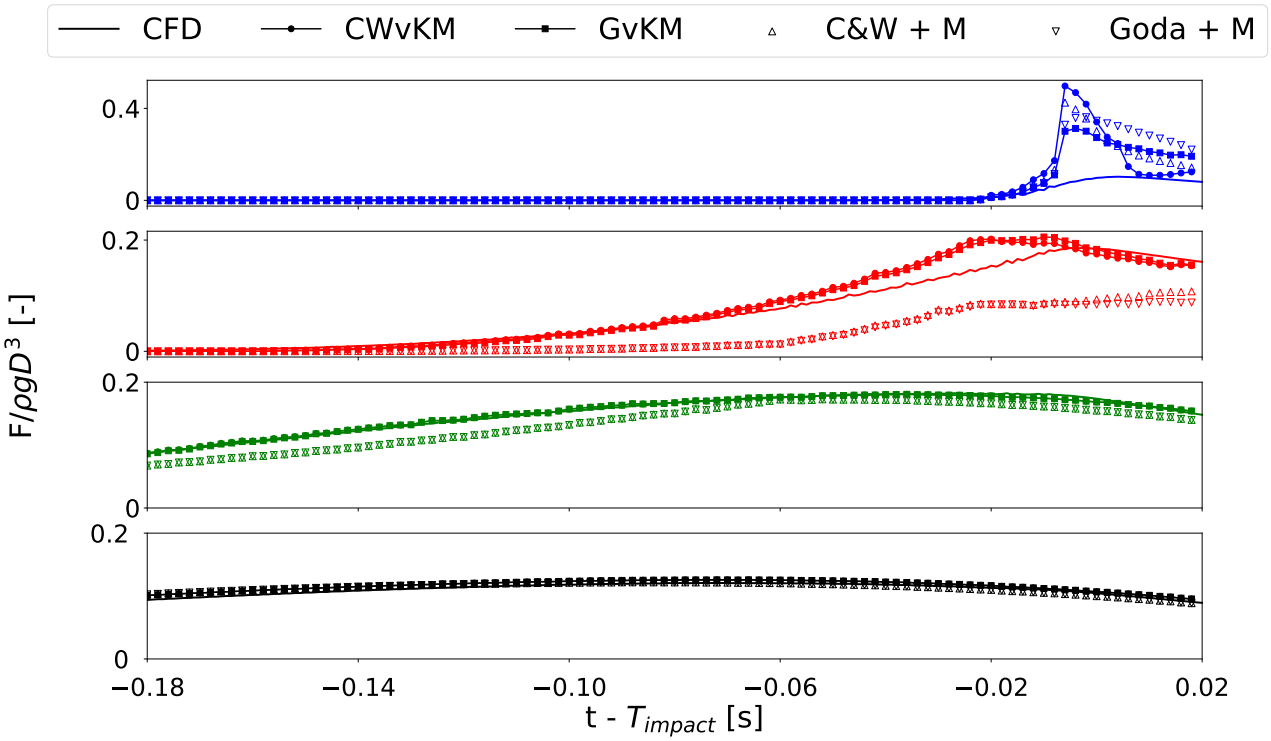

Figure 8: Time history of the load decomposed by section for case A4. From top to bottom: section 1 to 4. Comparison between CFD results (line) and semi-analytical results: CWvKM (circles), GvKM (squares), Campbell & Weynberg formula + Morison equation (C&W + M, upward triangles), Goda formula + Morison equation (Goda + M, downward triangles).

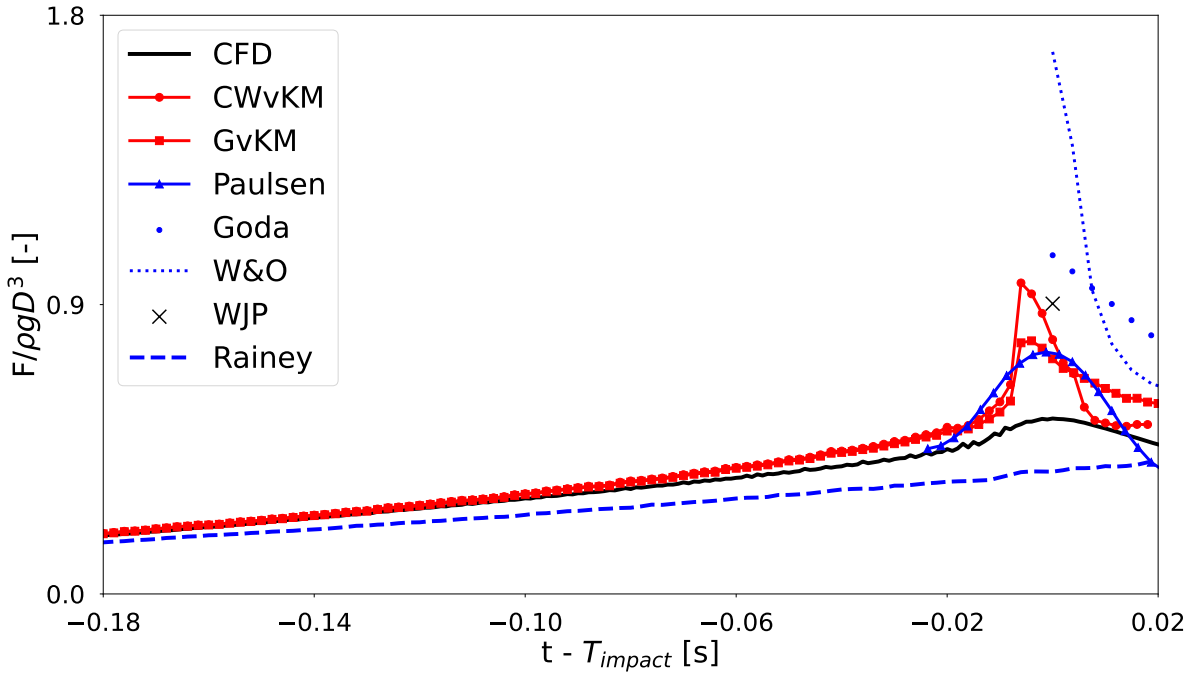

Figure 9: Time history of the total load for case A4. Comparison between CFD results (line) and semi-analytical results: CWvKM (red circles), GvKM (red squares), Paulsen (blue triangles), Goda (blue dots), W&O (blue dotted line), WJP (black cross) and Rainey (blue dashed line).

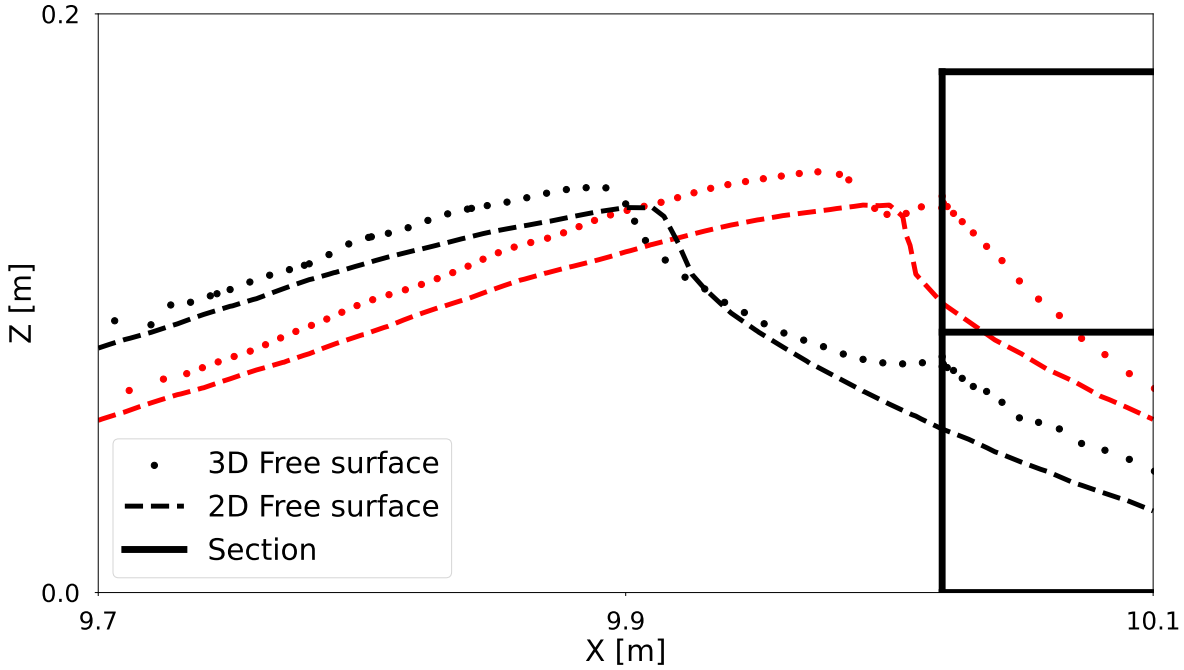

Figure 10: Comparison of the 2D (dotted line) and 3D (circles) free surface at t = 20.312 s (black marks) and t = 20.368 s (red marks) for case A4.

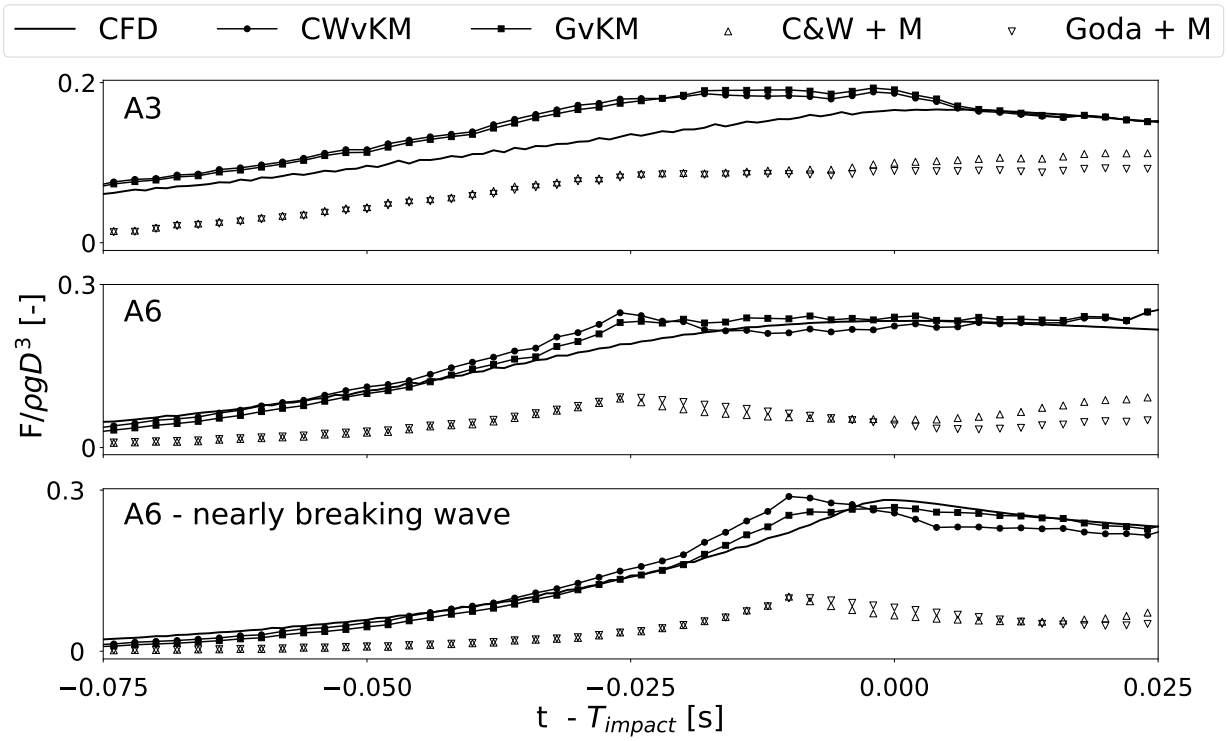

Figure 11: Time history of the load in section 2. From top to bottom: case A3, A6 and A6 - nearly breaking wave. Comparison between CFD results (line) and semi-analytical results: CWvKM (circles), GvKM (squares), Campbell & Weynberg formula + Morison equation (C&W + M, upward triangles), Goda formula + Morison equation (Goda + M, downward triangles).

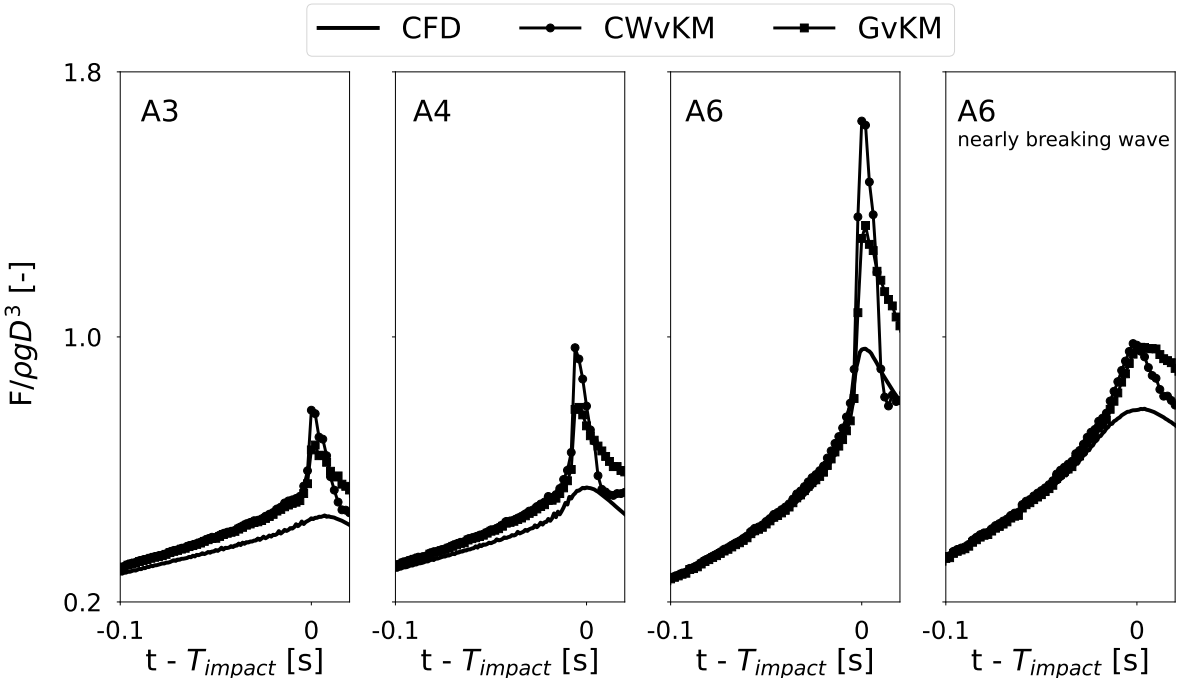

Figure 12: Time history of the total load. From left to right: case A3, A4, A6 and A6 - nearly breaking wave. Comparison between CFD results (line) and semi-analytical results: CWvKM (circles), GvKM (squares).

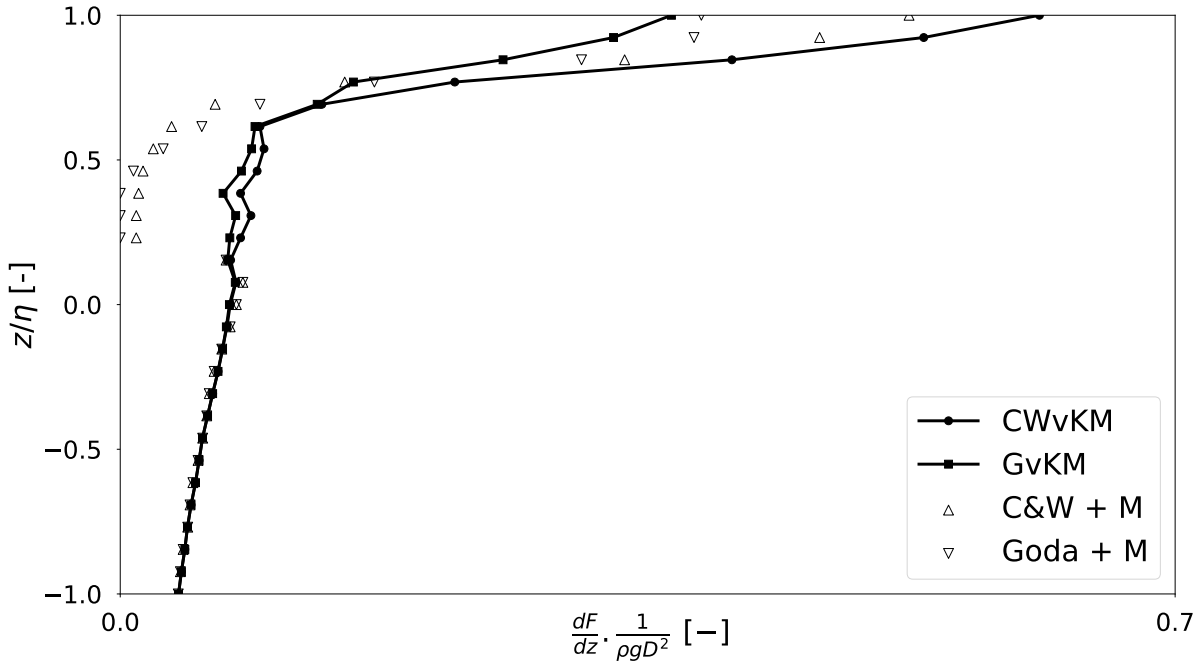

Figure 13: Force distribution profile at the time of maximum total load for case A4. Comparison between CWvKM (circles), GvKM (squares), Campbell & Weynberg formula + Morison equation (C&W + M, upward triangles), Goda formula + Morison equation (Goda + M, downward triangles).

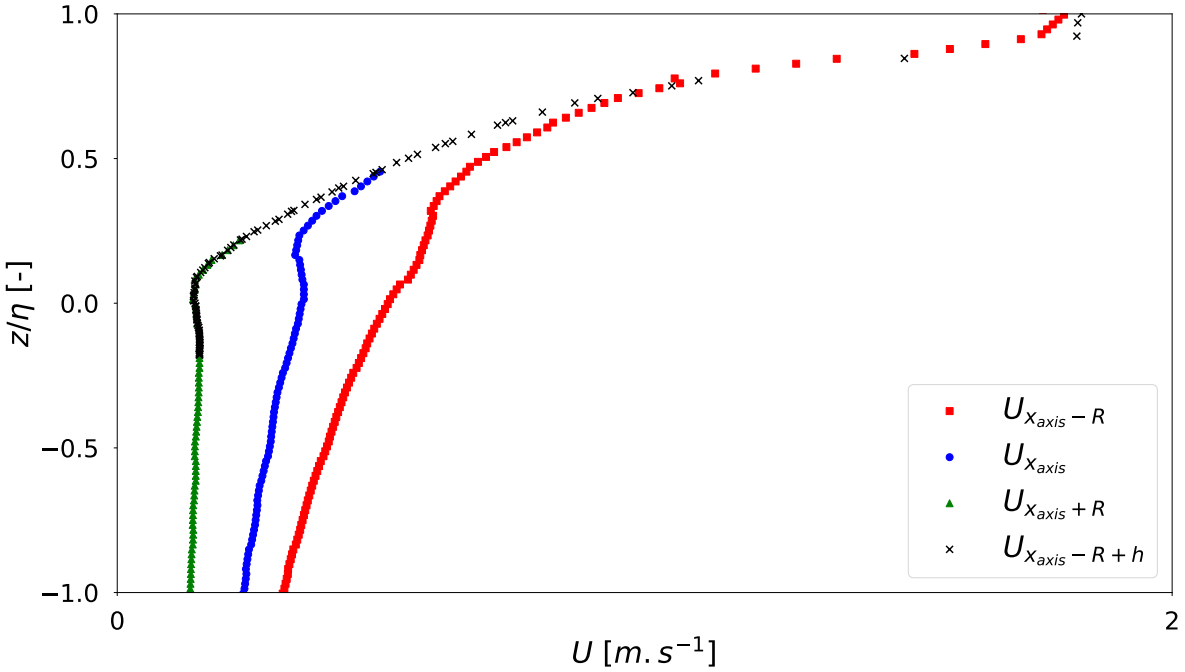

Figure 14: Horizontal velocity distribution profile at the time of maximum total load for case A4. Horizontal velocity at $x_{axis} - R$ ($U_{x_{axis}-R}$, red squares), x_{axis} ($U_{x_{axis}}$, blue dots), $x_{axis} + R$ ($U_{x_{axis}+R}$, green triangles) and at the free surface ($U_{x_{axis}-R+h}$, black crosses).

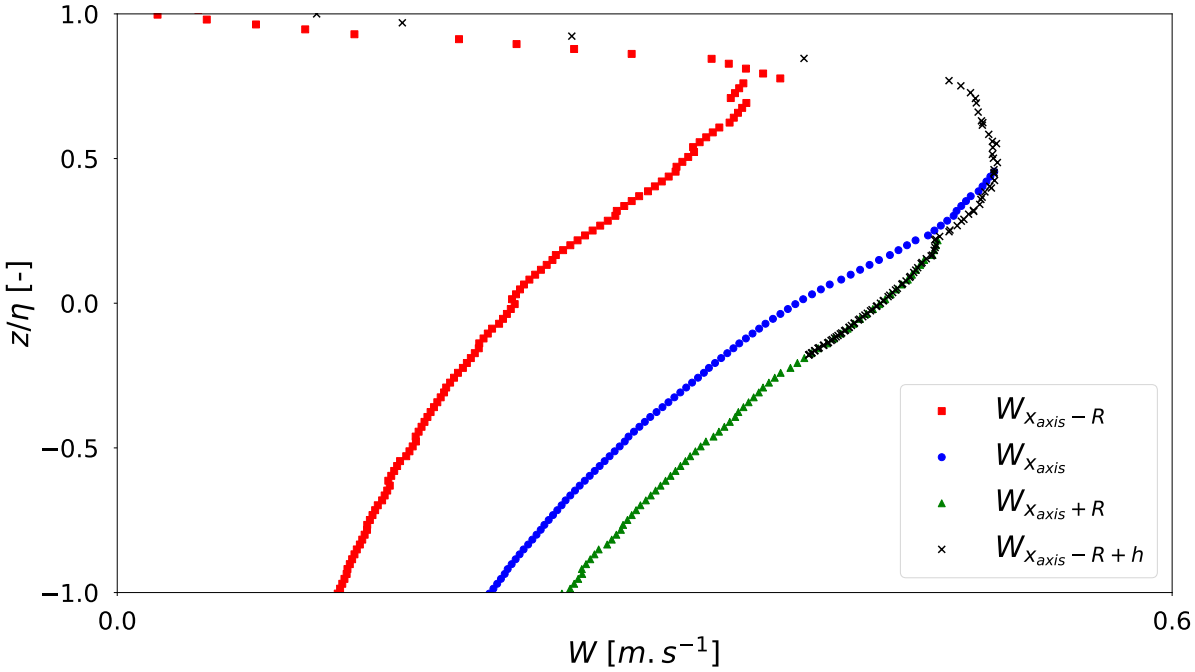

Figure 15: Vertical velocity distribution profile at the time of maximum total load for case A4. Vertical velocity at $x_{axis} - R$ ($W_{x_{axis}-R}$, red squares), x_{axis} ($W_{x_{axis}}$, blue dots), $x_{axis} + R$ ($W_{x_{axis}+R}$, green triangles) and at the free surface ($W_{x_{axis}-R+h}$, black crosses).